

ESTIMATING NEAR-SURFACE SOIL MOISTURE USING ACTIVE MICROWAVE SATELLITE IMAGERY AND OPTICAL SENSOR INPUTS

J. M. S. Hutchinson

ABSTRACT. Recent advances in radar remote sensing techniques illustrate the potential for monitoring soil moisture conditions at spatial and temporal scales required for regional and local modeling efforts. This research examined the feasibility of producing accurate and spatially distributed estimates of soil moisture using a time series of ERS-2 radar images for a tallgrass prairie ecosystem in northeast Kansas. Methods used included field data collection of soil moisture, digital image interpretation of optical (NOAA AVHRR and LANDSAT TM) and radar (ERS-2) imagery, and environmental modeling in a raster geographic information system (GIS) and image processing environment. Critical to this study was determining the scattering behavior of overlying vegetation, or the contribution of vegetation backscatter (σ_{veg}^o) to the total backscatter coefficient (σ_{total}^o), which was simulated using a modified water cloud model. By removing σ_{veg}^o from σ_{total}^o , the amount of backscatter contributed by the soil surface (σ_{soil}^o) was isolated and the linear relationship between σ_{soil}^o and volumetric soil moisture determined. Single-date correlations averaged $r = 0.62$ and $r = 0.67$ for a burned and unburned watershed, respectively, within the study area. While previous studies have questioned the sensitivity of C-band radars to near-surface soil moisture conditions, these results show that ERS-2 data may be capable of monitoring soil moisture conditions over even extremely dense natural grassland vegetation.

Keywords. Grasslands, Models, Radar, Remote sensing, Soil water, Soil water content.

Radar remote sensing is increasingly being used as a tool to collect environmental and natural resource information. The measurement of biophysical variables, such as near-surface soil moisture, is possible through quantification of the backscatter coefficient (σ^o), a complex value representing the cumulative impact of several factors that determine the reflectivity of different illuminated surfaces in the microwave spectrum.

Impacts of radar system parameters and landscape characteristics on σ^o are interrelated and should be considered in terms of their geometric and electrical control over microwave scattering. Geometric controls are largely related to image geometry and include the influence of structural attributes of Earth surface features such as vegetation. Electrical controls are determined by the relative dielectric constants of illuminated soil and vegetation at a given microwave wavelength. While geometric factors shape the three-dimensional distribution of the scattered field, electrical properties help to determine the magnitude of the radar backscatter response (Dobson et al., 1995).

With the presence of a vegetation canopy, radar backscatter consists of energy returned to the sensor from four types of target interactions: direct scattering (volume scattering),

reflection and direct reflection (surface-volume), and surface scattering (Chauhan et al., 1994; Engman and Chauhan, 1995). These interactions act to reduce the amount of backscattered energy while increasing the vegetation information content within the backscattered signal (e.g., canopy moisture status). At incidence angles near nadir, σ^o is dominated by the surface scattering component; hence, embedded soil moisture information is derived from the soil surface directly. However, at larger incidence angles, the canopy volume and surface-volume components increase in importance (Fung and Eom, 1985). Given the incidence angles of current operational synthetic aperture radar (SAR) satellites, the backscatter contribution of vegetation canopies is likely of enough significance to require a correction factor in order to extract accurate soil moisture estimates (Cognard et al., 1995).

The foundation of radar-based soil moisture investigations is the linear relationship between σ^o and volumetric soil water content (θ_v) in the upper 5 cm of the soil profile (Dobson and Ulaby, 1986; Pultz et al., 1990; Lin et al., 1994; Engman and Chauhan, 1995). However, successful near-surface soil moisture estimation requires isolating that amount of backscatter containing information from the surface of interest. Simulation models have been and are currently being developed to better understand interactions between radar energy and the complex land cover of the Earth's surface (Fung et al., 1992; Saatchi et al., 1994). Models such as these, based on a series of complex mathematical computations, provide a means to assess environmental change and, in doing so, offer insight into whether that change originated from natural variability or human alteration of the environment (Steyaert, 1993).

Article was submitted for review in September 2001; approved for publication by the Soil & Water Division of ASAE in December 2002.

The author is **J. M. Shawn Hutchinson**, Assistant Professor, Department of Geography, Kansas State University, 118 Seaton Hall, Manhattan, KS 66506; phone: 785-532-6727; fax: 785-532-7310; e-mail: shutch@ksu.edu.

MATERIALS AND METHODS

The objective of this study was to develop a process for, and determine the feasibility of, generating accurate and spatially distributed estimates of near-surface soil moisture using a time series of spaceborne SAR images. To accomplish this, a simulation model was developed to estimate the contribution of backscattered radar energy from vegetated surfaces (σ_{veg}^0) to total radar return (σ_{total}^0). A multi-sensor technique using normalized difference vegetation index (NDVI) from the Advanced Very High Resolution Radiometer (AVHRR) and LANDSAT Thematic Mapper (TM) sensors was applied to generate aboveground vegetation biomass data for input into the simulation model. By modeling the vegetative contribution to the total amount of backscattered radar energy, the amount of microwave energy scattered only by the soil surface (σ_{soil}^0) could then be estimated. Finally, the linear relationship between σ_{soil}^0 and θ_v was described to determine whether the two terms could be inverted in order to quantify near-surface soil moisture conditions across the study area and over time.

STUDY AREA

The relationship between radar backscatter and soil moisture was examined at the Konza Prairie Biological Station (KPBS), a 3487 ha site located approximately 11 km south of Manhattan, Kansas, within the northern reaches of the Kansas Flint Hills (fig. 1). The original 371 ha of what was to become Konza Prairie was purchased by The Nature Conservancy in 1971 and then deeded to Kansas State University (Knapp and Seastedt, 1998). Managed by the Division of Biology at Kansas State University, Konza now represents the largest, and one of the most intensively studied, portion of tallgrass prairie in North America dedicated to ecological research.

An experimental plan established in 1971 assigned KPBS watersheds to different management treatments of prescribed fire ranging from annual burns to long-term fire exclusion (e.g., 20 years). In October 1987, bison were reintroduced to Konza to examine the effects of grazing on the prairie ecosystem and, as of 1992, 1100 ha were being actively grazed. Cattle also graze in selected watersheds. In 1980, Konza was chosen as one of six original long-term ecological research (LTER) sites funded by the National Science Foundation (NSF) and was included as the site of intensive field campaigns related to NASA's First International Satellite Land Surface Climatology Project (ISLSCP) Field Experiment (FIFE) in 1987 and 1989.

IMAGE PRE-PROCESSING

A time-series of seven precision image (PRI) SAR products from the second European Remote Sensing Satellite (ERS-2) were acquired during the summer and fall of 1996

(table 1). These images were processed by the European Space Research Institute (ESRIN) in a speckle-reduced (i.e., multiple look) format and corrected for SAR antenna pattern and range-spreading loss. Operating characteristics of the ERS-2 satellite are listed in table 2.

The complete set of images was composed of two subsets of four ascending and three descending repeat-pass images. Each subset of images was co-registered using a first-order transformation to better align the images and then combined into image stacks. Each image stack was then subjected to an image-to-map registration process using a third-order polynomial transformation and no fewer than 10 ground control points (GCPs) to convert GCP file coordinates to Universal Transverse Mercator (UTM) coordinates (ERDAS, 1994). After the images were registered and geocoded, the two image stacks were combined into a single seven-image raster stack. A GIS containing a vector file of the KPBS boundary was then used to clip the study area from the radar image stack.

In ERS-2 PRI images, the digital number (DN) values do not represent varying magnitudes of the backscatter coefficient (σ^0). Rather, pixel intensities are representative of the radar brightness (β^0) of illuminated scenes. Laur et al. (1998) describes the relationship between β^0 and σ^0 within a radar image. The conversion of image DN values to corresponding σ^0 requires knowledge of pixel-specific local incidence angles. To estimate this parameter, slope and aspect (relative

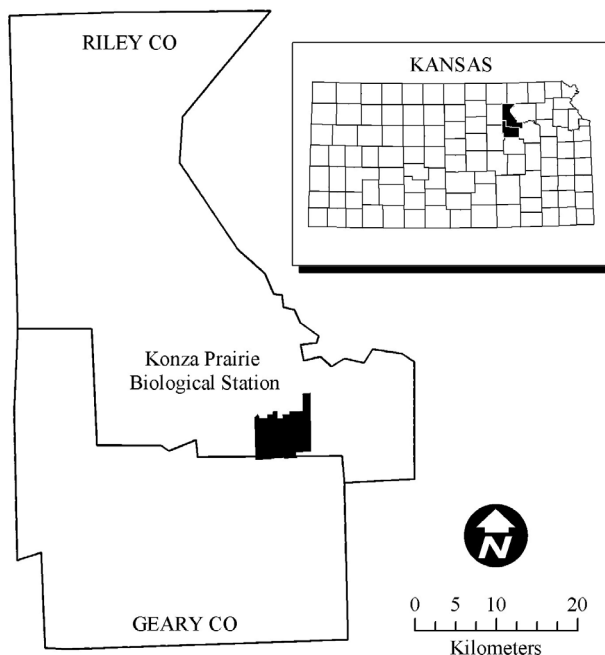


Figure 1. Location of Konza Prairie Biological Station (KPBS), a tallgrass prairie site in northeastern Kansas (Riley and Geary County).

Table 1. Acquired ERS-2 images for the KPBS study area during the summer and fall of 1996 (acquisition times are CST, look direction is in degrees, A = ascending pass, and D = descending pass).

| Information | 23 July | 1 August | 27 August | 5 September | 1 October | 10 October | 5 November |
|------------------|---------|----------|-----------|-------------|-----------|------------|------------|
| Orbit | 6572 | 6708 | 7073 | 7209 | 7574 | 7710 | 8075 |
| Frame | 0783 | 2817 | 0783 | 2817 | 0783 | 2817 | 0783 |
| Path | 205 | 341 | 205 | 341 | 205 | 341 | 205 |
| Pass direction | A | D | A | D | A | D | A |
| Acquisition time | 2342 | 1212 | 2342 | 1212 | 2342 | 1212 | 2242 |
| Look direction | 75.9 | 283.9 | 75.9 | 283.9 | 75.9 | 283.9 | 75.9 |

Table 2. ERS-2 satellite operating characteristics (from Kramer, 1996).

| Satellite | ERS-2 |
|---------------------|--------------------------|
| Operational date | 21 April 1995 to current |
| Sensor | AMI (C-band SAR) |
| Wavelength | 5.66 cm |
| Polarization | VV |
| Look angle | 23° |
| Spatial resolution: | 30 × 30 m |
| Altitude | 780 km |
| Swath width | 100 km |

to northing) information were derived from a 7.5 minute USGS digital elevation model (DEM) of the study area. This topographic information was combined with the known value for the sensor depression angle ($\theta_d = 67^\circ$) to develop a raster layer of local incidence angles (θ_i) on a per-pixel basis (Goyal et al., 1998).

The DN conversion process also requires the calibration constant (K) specific to the sensor and processing center that can be found in the SAR leader file, one of four header files that accompany each PRI image (see Appendix D of Laur et al., 1998). Image DN values, in backscatter coefficient form, were then converted into decibel (dB) units (Laur et al., 1998).

TOPOGRAPHIC CORRECTION OF RADAR IMAGES

Before the relationship between σ_{soil}^0 and θ_v could be quantified, the “topographic effect” of variable terrain that is readily apparent in active microwave images had to be minimized (i.e., image restoration). Undulating terrain produces significant radiometric variations throughout a radar scene due to the active nature of the sensor and its direct effect on sensor-target geometry. The effect of relief on SAR imagery can be significant and may be confused with variance caused by vegetation and soil conditions. Bayer et al. (1991) estimate that between 14% and 40% of DN variance in SAR images may be attributed to variations in topography.

Five topographic variables, local incidence angle (LIA), aspect relative to northing (AS), aspect relative to radar look direction (AR), slope (SL), and elevation (EL), were examined using correlation analysis to determine which was most closely related to σ_{total}^0 . That topographic variable was then used in a polynomial equation designed to minimize the impact of that variable on the magnitude of σ_{total}^0 values. This polynomial equation forms the basis for the derivation of an empirical correction function that has been shown effective at reducing terrain-induced DN variance over agricultural landscapes (see Bayer et al., 1991, for a complete description of the topographic correction technique).

CLOUD MODEL DESIGN

A general first-order model describes the components of the total amount of backscattered radar energy (σ_{total}^0) recorded on a SAR image (Ulaby et al., 1982):

$$\sigma_{total}^0 = \sigma_{veg}^0 + (\sigma_{soil}^0 / L^2) \quad (1)$$

where

- σ_{total}^0 = total amount of radar backscatter
- σ_{veg}^0 = backscatter contributed by vegetation
- σ_{soil}^0 = backscatter contributed by soil surface
- L^2 = two-way loss factor of the vegetation canopy.

The total amount of radar backscatter (σ_{total}^0) is a known quantity represented by the calibrated and converted DN values in the SAR PRI images. The two-way loss factor (L^2) is the squared value of the one-way (one direction) loss factor (L) (Ulaby et al., 1982):

$$L = \exp(\kappa_e \times h \times \sec\theta) \quad (2)$$

where

- κ_e = volume extinction coefficient
- h = vegetation canopy height
- θ = sensor incidence angle (23°)

The three-dimensional distribution of water molecules at the Earth’s surface exerts primary control over the behavior of microwave energy (Dobson et al., 1995). For most of these surfaces, vegetation and the uppermost layers of the soil profile control both the distribution and the abundance of water. A simple cloud model, first introduced by Attema and Ulaby (1978), estimates σ_{veg}^0 by simulating the vegetation canopy as a dense “cloud” of water particles or droplets (Ulaby et al., 1982):

$$\sigma_{veg}^0 = [(\sigma_v \times \cos\theta) / 2\kappa_e] \times (1 - 1 / L^2) \quad (3)$$

where σ_v = volume backscattering coefficient.

By simulating vegetation as a water cloud, the canopy volume is assumed to consist of randomly distributed uniform scatterers. Here, the effect of multiple scattering was ignored. This approach greatly simplifies the multiple calculations that are required to recreate the scattering environment at the time the SAR imagery was acquired. Once σ_{veg}^0 is determined, equation 1 may be rearranged, solved for σ_{soil}^0 , and compared to field measurements of soil moisture.

CLOUD MODEL PARAMETERIZATION

Input variables required by the cloud model equations for use in the first-order backscatter model fall into three categories (table 3). The first category is fixed system parameters related to SAR sensor operating characteristics. These system variables may be the most critical for successful soil moisture estimation, as microwave wavelength (λ) and incidence angle (θ) play a large role in

Table 3. Required input variables for cloud model processing.

| Category | Variables | Symbol | Units |
|-------------|-------------------------------------------------------|-----------|--------------|
| System | Incidence angle | θ | degrees |
| | Microwave wavelength | λ | cm |
| Vegetation | No. of scattering particles per unit of canopy volume | N | No. m^{-3} |
| | Canopy height | h | m |
| Water cloud | Radius of water cloud particle | r | cm |
| | Real part of dielectric constant | K | |
| | Imaginary part of dielectric constant | Im (-K) | |

determining the attenuation of incoming microwave energy from vegetation interactions.

The second category of input variables consists of the vegetation parameters canopy height (h) and number of scattering particles per unit of canopy volume (N). Green canopy height was set at 0.46 m for the entire study area based on measured canopy values reported in Saatchi et al. (1994). The number of scattering particles per unit volume (N) was derived from estimates of aboveground net primary production (ANPP) for the study area (see the following section) and is dependent on the size of water particles used to simulate both living (green) and dead plant biomass. As ANPP changes over time and space, the number of water particles required to simulate biomass must also change. The three-dimensional space occupied by the water cloud (i.e., canopy volume) is defined in length and width by the size of the radar image pixel (30×30 m) and in height by the canopy (h).

The final category of variables describes properties of the water cloud used to simulate the vegetation canopy, specifically the water droplet radius (r) and dielectric properties of the vegetation (K). A dielectric constant of $15 + i5.5$ for a green plant canopy (at C-band wavelengths) was taken from Saatchi et al. (1994), who calculated the value using the Ulaby–El Rayes procedure applied to plant moisture and biomass measurements taken during FIFE. For water droplets simulating plant litter in unburned watersheds, a dielectric constant of $74.0 + i26.2$ (again at C-band) was adopted, as determined by Saatchi et al. (1994) using the Debye formula for pure water.

Water droplet size (r) impacts simulated σ_{veg}^0 values in several ways. First, larger droplet sizes result in more backscatter from the vegetation canopy at a given biomass amount, and a greater rate of change in the magnitude of σ_{veg}^0 as scattering particle density, or biomass, increases. In

addition, the amount of radar energy lost through extinction within the scattering volume or scattering away from the sensor is closely related to the dimensions of the water droplet.

The scattering behavior of water droplets with radii of 0.5 to 1.5 cm was simulated in a spreadsheet, programmed with the equations described earlier, over a range of ANPP levels (0 to 1000 g m^{-2}) possible for tallgrass prairie. These simulations showed that a droplet radius of 1.0 cm for green biomass resulted in the most reasonable contributions to σ_{total}^0 from σ_{veg}^0 given minimum ($231.2 \pm 18.6 \text{ g m}^{-2}$) to average ($417.1 \pm 18.7 \text{ g m}^{-2}$) through maximum ($589.9 \pm 24.6 \text{ g m}^{-2}$) ANPP for the study site, as measured during the period 1975–1996 (Knapp et al., 1998). The 1.0 cm radius droplets showed the greatest change in σ_{veg}^0 over 200 to 500 g m^{-2} ANPP levels and dominated total backscatter (σ_{total}^0) at the highest production levels (fig. 2).

From the perspective of radar remote sensing, presence of a litter layer in some grassland areas can have a significant impact on backscatter magnitude, especially if the layer is thick and/or holds large amounts of water. Knapp et al. (1998) reported that litter layers in KPBS can accumulate over time to amounts approaching 1000 g m^{-2} , or a depth of 30 cm, in highly productive areas.

A similar justification applies for the selection of a 0.75 cm droplet radius to represent dead vegetation in accumulated litter layers of unburned watersheds. References to “litter layer” here includes only the thick mat of dead vegetation found near the soil surface, not standing dead biomass generated annually. Since 1990, research at KPBS shows that biomass production in both upland and lowland areas has generally exceeded the long-term mean values (Knapp et al., 1998). For this reason, litter biomass in this study was set at 450 g m^{-2} , rather than the $382 \pm 19 \text{ g m}^{-2}$

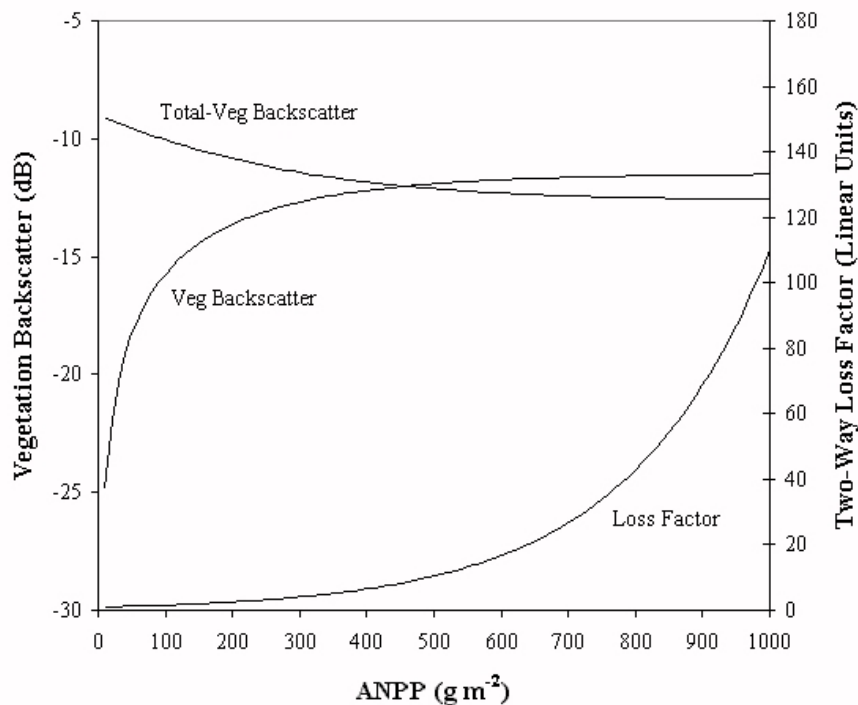


Figure 2. Cloud model simulation results showing the impact of vegetation on the quantity of $\sigma_{total}^0 - \sigma_{veg}^0$ for a particle radius of 1.0 cm (assumes $\sigma_{total}^0 = -9.0$ dB).

average reported by Briggs et al. (1998). This total results in the litter layer contributing a constant -18.7 dB to the total backscattered signal, with a two-way loss value of 1.9 linear units (m m^{-1}).

The cloud model for unburned sites differs from that of burned areas, as it consists of two distinct layers rather than one consisting of the plant canopy alone, as presented in equation 1. In the two-layer model, contributions of the plant canopy and litter layer are assumed to be additive and must also be modified to account for backscatter contributions and loss factors of the two types of scattering media:

$$\sigma_{\text{soil}} = [(L_1^2 + L_2^2) \times \sigma_{\text{total}}] - (\sigma_{\text{veg}} \times L_1^2) - (\sigma_{\text{litter}} \times L_2^2) \quad (4)$$

where

L_1 = two-way loss factor of the vegetation canopy

L_2 = two-way loss factor of the litter layer

σ_{litter} = backscatter contribution of the litter layer.

Litter backscatter calculations are performed using the same formulas (eqs. 3 and 4) used for σ_{veg} , changing only water droplet size and substituting an average litter layer thickness ($h = 0.1$ m) for green canopy height.

STUDY AREA DELINEATION

The remaining variable to be quantified in order to successfully derive soil-contributed backscatter (σ_{soil}) is the number of scattering particles per unit volume (N). Given the temporal dimension of this study, using only a single biomass estimate such as peak ANPP, which is routinely measured through the Konza LTER program, was not considered appropriate. Single measurements fail to account for variations in ANPP that have been shown to exist within the study area over both space and time. Therefore, it was necessary to subset KPBS into areas of similar biomass characteristics in order to calculate more realistic N values.

Given consistent and significant differences in ANPP between burned and unburned sites in years with normal precipitation (Knapp et al., 1998) and the sensitivity of microwave energy to the presence of a litter layer, fire frequency was used as the basis for study area differentiation. The question then became one of determining the appropriate fire frequency to use in distinguishing between a “burned” and “unburned” watershed. Because an equilibrium between the accumulation and decomposition of litter is reached in approximately three years in tallgrass systems (Knapp et al., 1998), “burned” watersheds were identified as those burned annually or every other year. All other watersheds were classified as “unburned” (fig. 3).

ABOVEGROUND BIOMASS ESTIMATION

Using vegetation indices derived from optical data acquired by other remote sensing platforms permits vegetation conditions to be characterized and evaluated throughout a growing season. When combined with point measurements taken on the ground, an index such as the normalized difference vegetation index (NDVI) can be very useful in inferring patterns and processes across a landscape (Goward, 1989; Jensen, 1983). Generic NDVI is a ratio of spectral bands that measures the “greenness” of the Earth’s surface (Rouse et al., 1974; Tucker, 1979):

$$\text{NDVI} = (\text{NIR} - \text{red}) / (\text{NIR} + \text{red}) \quad (5)$$

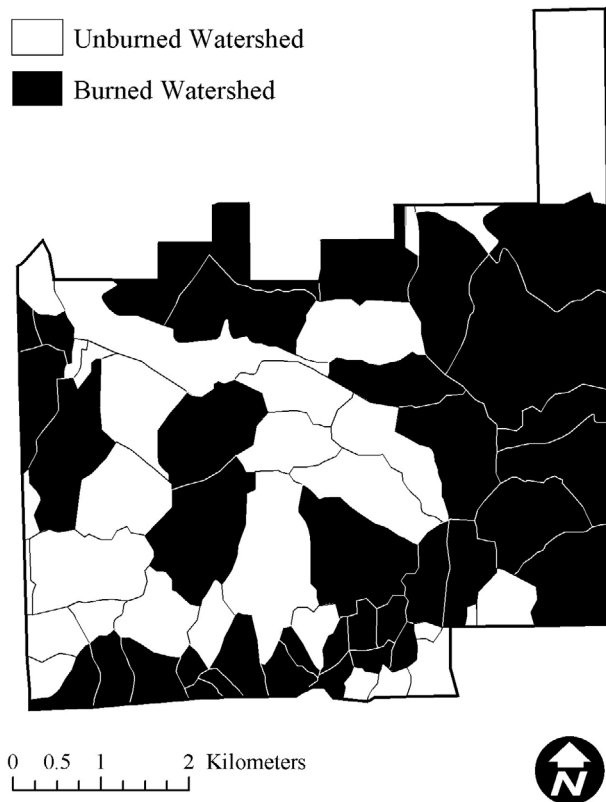


Figure 3. Delineation of the KPBS study area by burning regime (as determined for this study).

where

NIR = near-infrared wavelength band (e.g., TM band 4)

red = red wavelength band (e.g., TM band 3).

The NDVI equation produces values in the range of -1.0 to 1.0 , where increasing positive values represent increasing greenness, and negative values indicate nonvegetated surface features (e.g., water, barren lands, ice and snow, or cloud cover). Empirical studies at KPBS, and elsewhere, have shown increasing greenness to be strongly related to aboveground biomass production (Briggs and Nellis, 1989; Goward et al., 1985; Norwine and Gregor, 1983; Tucker et al., 1985; Tucker et al., 1991; Townshend and Justice, 1986; Yang et al., 1997).

For this study, optical data from two different satellite sensors were used to calculate NDVI and estimate biomass production during the study period. The first data were biweekly maximum NDVI composites of the U.S. based on imagery from the Advanced Very High Resolution Radiometer (AVHRR), one of several sensors onboard the improved TIROS series of meteorological satellites operated by the National Oceanographic and Atmospheric Administration (NOAA). Compositing periods are necessary to minimize the impact of cloudy conditions on AVHRR observations of the land surface. The result is a nearly cloud-free image that depicts maximum vegetative greenness during the composite period (Eidenshink, 1992).

A total of eleven biweekly NDVI composites spanning the study period were used to calculate mean NDVI values for the entire study area (table 4). Mean NDVI values from each composite period were assigned a midpoint date so that a line could be fit between data points to estimate NDVI on days when biomass clipping occurred (fig. 4). The advantage of

Table 4. Biweekly AVHRR NDVI composite periods used in this study.

| Biweekly Period | Date of Coverage (1996) | | Day of Year (DOY) | Period Midpoint (DOY) |
|-----------------|-------------------------|----------|-------------------|-----------------------|
| | From | To | | |
| 13 | 21 June | 4 July | 173–186 | 179 |
| 14 | 5 July | 18 July | 187–200 | 193 |
| 15 | 19 July | 1 Aug. | 201–214 | 207 |
| 16 | 2 Aug. | 15 Aug. | 215–228 | 221 |
| 17 | 16 Aug. | 29 Aug. | 229–242 | 235 |
| 18 | 30 Aug. | 12 Sept. | 243–256 | 249 |
| 19 | 13 Sept. | 26 Sept. | 257–270 | 263 |
| 20 | 27 Sept. | 10 Oct. | 271–284 | 277 |
| 21 | 11 Oct. | 24 Oct. | 285–298 | 291 |
| 22 | 25 Oct. | 7 Nov. | 299–312 | 305 |
| 23 | 8 Nov. | 21 Nov. | 313–326 | 319 |

AVHRR-based NDVI data is that it is a low-cost source of temporal vegetation information, including primary productivity and biomass (Box et al., 1989). However, the coarse spatial resolution of the AVHRR sensor (approximately 1 × 1 km pixel resolution) precludes estimating biomass at a level of detail sufficient for input into the cloud model. Because of this, a single LANDSAT 5 Thematic Mapper (TM) image (30 × 30 m pixel resolution) was used to spatially extend the greenness trend information provided by the AVHRR time-series.

A single TM image from 22 July 1996 was acquired and used to calculate NDVI for the study area (eq. 5). It was assumed that landscape conditions captured by the TM image were the same for 23 July, the initial radar image acquisition date, and 24 July, the first day for which biweekly biomass measurements were available through LTER sampling activities. Using estimated mean AVHRR NDVI from 24 July as the base, TM NDVI values were adjusted linearly based on percent change in mean AVHRR NDVI values, so that vegetation index information of greater spatial resolution could be forecasted for the remaining clipping dates and

throughout the entire study period. Scaling the AVHRR data in this manner is justified given that the study area flora is dominated by relatively few species of perennial warm-season grasses that display similar phenological development throughout the growing season (Freeman, 1998; Briggs et al., 1998).

Next, the mean TM NDVI for watersheds 1A and 20A, a burned and unburned watershed where biweekly biomass sampling was conducted, was determined and used to develop a linear regression model relating the AVHRR-modified TM NDVI values to aboveground net primary production (ANPP). Figure 5 illustrates how delineation of the study area by burning treatment, aboveground biomass estimates, and the various components of the radar cloud model interact to generate soil backscatter (σ_{soil}^0) values.

Burned watersheds lack the accumulated litter found in unburned watersheds and differ in the amount of aboveground production. Remotely sensed ANPP estimates provide a means to identify the spatial and temporal variation in aboveground biomass that, after cloud model processing, impacts the magnitude of σ_{veg}^0 and the resulting σ_{soil}^0 value. This relationship is repeated within unburned watersheds, with the added influence of a litter layer, by describing litter in a similar manner as the green plant canopy (e.g., height, biomass, dielectric constant) and processing this information using the appropriate cloud model equations.

SOIL MOISTURE SAMPLING

Soil samples were collected along two transects spanning an upland-lowland-upland topographic gradient in both an annually burned (1D) and unburned (20B) watershed (fig. 6). For ascending-pass images, soil sampling occurred the morning following satellite overpass, approximately eight hours after image acquisition. For descending-pass images, sampling occurred about two hours prior to actual overpass time (table 1).

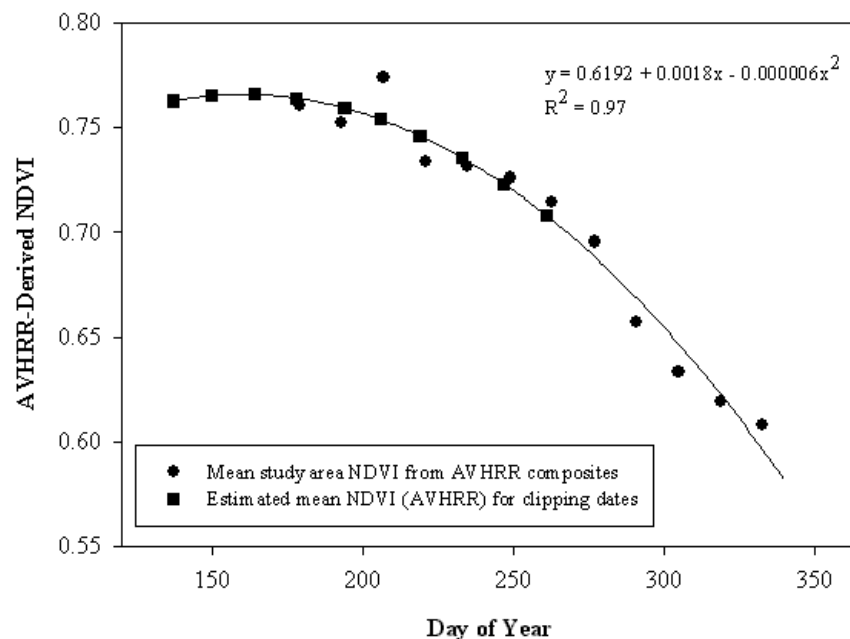


Figure 4. Mean and estimated mean AVHRR-derived NDVI values for KPBS (1996).

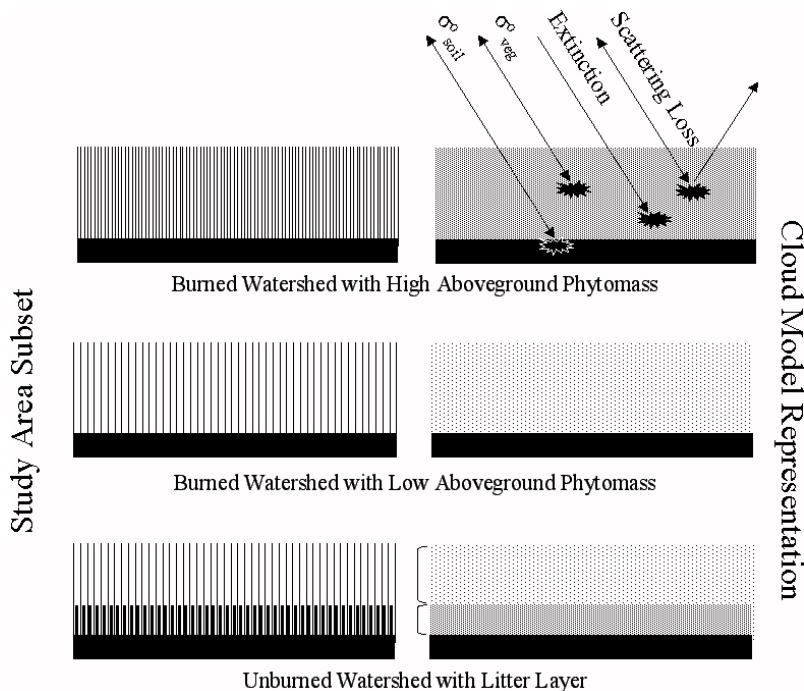


Figure 5. Conceptual diagram of the cloud model illustrating differences between burned and unburned vegetated surfaces.

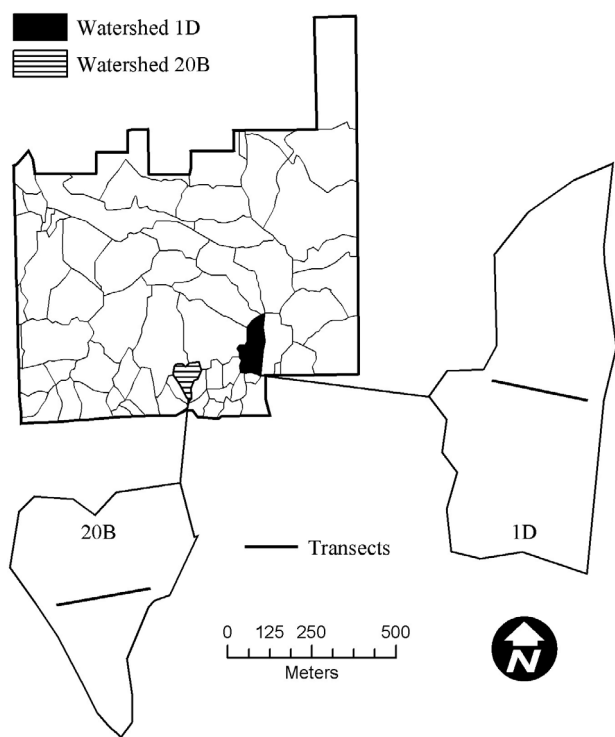


Figure 6. Location of transects and soil sampling points in watershed 1D (burned) and 20B (unburned).

During each collection period, 12 soil samples were extracted from the top 5 cm of the soil profile at each of 11 locations along both transects. To minimize possible error caused by small-scale soil variations, the 12 samples collected at each point were averaged to generate a single soil moisture measurement. After extraction, the soil samples were placed in a chilled cooler and transported to laboratory facilities, where a series of weight measurements were taken.

The first measurement included the plastic bag and soil plugs. After weighing, the soil samples were removed from the plastic bags, placed into paper containers, and oven-dried at 110 °C for three days. The empty plastic bags were then re-weighed. After oven-drying, the soil samples were weighed once more in their paper containers, emptied, and the paper containers re-weighed.

Mass wetness (w), or gravimetric water content on a percentage basis, was then calculated. Gravimetric soil moisture measurements were converted to volumetric water content (θ_v) by assuming a bulk density of 1 g cm⁻³, as volumetric measurements are more commonly associated with σ^0 values. Although measures of bulk density at each sample location may have improved the correlation with σ^0 , these data were not available. However, the bulk density assumption made here is supported by measurements taken throughout the study area during FIFE, where average bulk density in the upper 25 mm of the soil profile was 1.008 g cm⁻³ (data obtained from FIFE website at: http://daac.ornl.gov/fife/fife_home.html).

RESULTS AND DISCUSSION

BIOMASS ESTIMATION

Estimates of aboveground biomass using NDVI data are most frequently performed during the period of green-up to peak biomass production. At KPBS, the relationship between ANPP and NDVI during this stage of phenological development is generally strong ($R^2 > 0.80$), but the slopes and y -intercepts of the regressions can vary significantly between years and watersheds (Briggs et al., 1998). Post-peak NDVI statistics are less frequently reported since the objective of much NDVI-related research is to estimate photosynthetically active aboveground vegetative biomass. Here, the post-peak biomass relationship with NDVI is a critical component for the success of the cloud model, with

biomass forming the basis from which the density of droplets in the water cloud was determined.

Separate regression models are required for burned and unburned watersheds, given the impact of accumulated litter on reflectance values. The importance of separate regression models based on fire regime may be even more critical as the vegetation begins to senesce, as steadily increasing amounts of dead, and standing dead, plant material likely influence reflectance to a greater extent than when the canopy is developing.

As expected, the explanatory power of the post-peak NDVI linear regression model is much greater for the annually burned watershed ($R^2 = 0.70$) than for the unburned watershed ($R^2 = 0.51$) (fig. 7). Although neither relationship was as strong as typical green-up values, the linear functions identified for watersheds 1A and 20A were used to estimate biomass throughout the study area. Given the importance of biomass in the cloud model process, the strength of the regression relationship has clear implications on the accuracy of σ_{soil} calculations and near-surface soil moisture estimates. Ideally, individual LANDSAT TM images (or other high spatial resolution imagery) acquired near clipping dates would be used to develop the regression equations. But given funding limitations for the purchase of additional satellite imagery, the kind of multi-sensor approach used to estimate biomass described in this exploratory study was a reasonably effective, and less expensive, alternative.

RADAR BACKSCATTER – SOIL MOISTURE RELATIONSHIPS

Examination of daily σ_{soil} -soil moisture relationships for both the burned and unburned watershed illustrates strengths and weaknesses of the modified cloud model approach for near-surface soil moisture estimation. Figure 8 (and table 5) shows correlations between σ_{soil} and volumetric soil moisture (θ_v) for 6 of 7 overpass dates within watershed 1D, the annually burned watershed (10 October was omitted due to soil moisture data collection problems). The correlation

coefficient for most (4 of 6) dates was greater than or equal to the mean of $r = 0.62$ (maximum of $r = 0.86$ on 27 August).

With the exception of 5 September, most image dates are tightly clustered in the two-dimensional space defined by σ_{soil} of -17 to 5 dB and θ_v of 27% to 53% . Despite being the driest ($\theta_v = 15\%$ to 29%) of all days for which radar imagery was acquired, σ_{soil} values were intermediate in magnitude compared to the other, wetter days. Because soil moisture conditions were very dry throughout most of the watershed, it is logical to assume that vegetation would experience water stress sufficient to lower canopy moisture content. However, in simulating σ_{veg} , the cloud model does not account for temporal changes in canopy moisture. If canopy moisture content were included in σ_{veg} calculations, it may have been possible to reduce estimated σ_{soil} , moving the 5 September data into a more comparable position (i.e., lower backscatter in fig. 8) compared to other image dates.

As with watershed 1D, correlations between σ_{soil} and θ_v for watershed 20B (unburned) were examined for 6 of 7 overpass dates (fig. 9 and table 5) (1 August was omitted due to soil moisture data collection problems). Five of the image dates show expected positive relationships between σ_{soil} and θ_v with correlation coefficients greater than or equal to $r = 0.54$ (maximum of $r = 0.79$ on 5 September). Soil backscatter and volumetric soil moisture had no relationship ($r = 0.00$) for the remaining image date (23 July).

Backscatter data from 23 July appear to have been affected by more than 30 mm of rain that fell on the previous day. Because fire had been excluded from this watershed, a litter layer was both present and very wet when the SAR image was acquired. Under these conditions, litter would have been reflecting maximum amounts of radar energy across the topographic gradient, dominating total backscatter and causing the flat relationship between σ_{soil} and soil moisture. As was the case with the 5 September data in watershed 1D, no moisture component for the litter layer was incorporated in the cloud model method. Instead, a constant

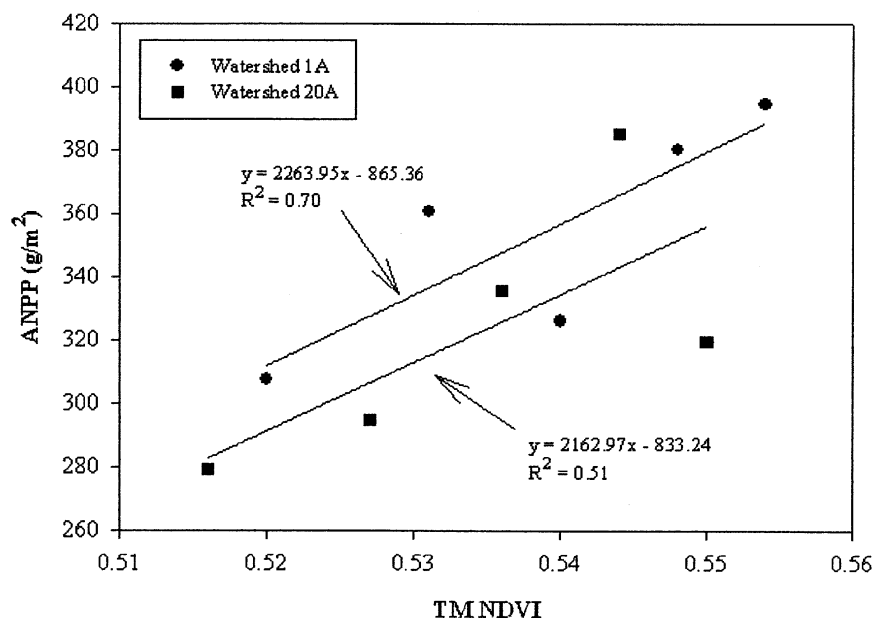


Figure 7. Relationship between ANPP and AVHRR-modified TM NDVI values for watersheds 1A (burned) and 20A (unburned).

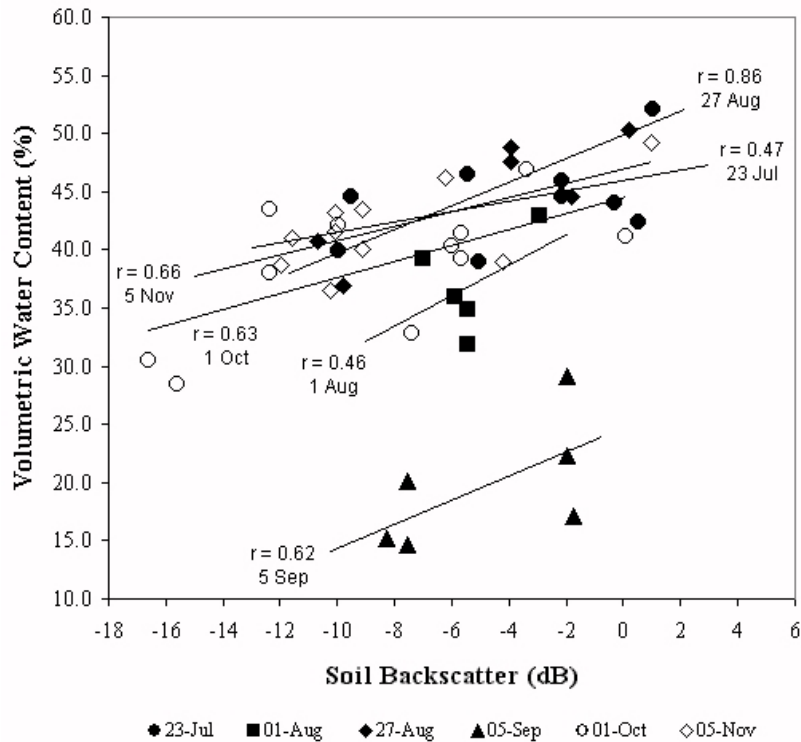


Figure 8. Correlations between soil backscatter (σ_{soil}^0) and volumetric soil moisture (θ_v) on watershed 1D (burned) for radar image acquisition dates (10 October 1996 not shown).

Table 5. Linear regression results for predicting volumetric soil moisture (θ_v) from soil-derived radar backscatter (σ_{soil}^0).

| Date (1996) | Water-shed | Slope | y Intercept | r | R ² | RSS | SE |
|-------------|------------|-------|-------------|------|----------------|-------|-------|
| 23 July | 1D | 0.45 | 45.95 | 0.47 | 0.22 | 24.76 | 9.36 |
| | 20B | -0.01 | 41.69 | 0.00 | 0.00 | 39.53 | 13.18 |
| 01 Aug. | 1D | 1.30 | 43.93 | 0.46 | 0.21 | 14.66 | 8.47 |
| | 20B | n/a | n/a | n/a | n/a | n/a | n/a |
| 27 Aug. | 1D | 1.01 | 49.89 | 0.86 | 0.74 | 13.07 | 6.54 |
| | 20B | 1.89 | 54.52 | 0.74 | 0.55 | 35.25 | 12.46 |
| 05 Sept. | 1D | 1.04 | 24.76 | 0.62 | 0.44 | 19.17 | 9.59 |
| | 20B | 1.15 | 32.96 | 0.79 | 0.62 | 24.70 | 9.34 |
| 01 Oct. | 1D | 0.69 | 44.56 | 0.63 | 0.40 | 38.76 | 12.92 |
| | 20B | 1.22 | 43.49 | 0.65 | 0.42 | 28.32 | 11.56 |
| 10 Oct. | 1D | n/a | n/a | n/a | n/a | n/a | n/a |
| | 20B | 1.52 | 40.50 | 0.61 | 0.37 | 51.11 | 18.07 |
| 05 Nov. | 1D | 0.62 | 46.92 | 0.66 | 0.38 | 22.87 | 8.09 |
| | 20B | 1.50 | 57.96 | 0.54 | 0.29 | 33.13 | 12.52 |

value of -18.7 dB for σ_{litter}^0 was used throughout the study period within the unburned areas. Excluding the 23 July date, mean correlation for the unburned watershed was $r = 0.67$.

Despite noted problems with the modified cloud model approach, single-date correlations for watershed 1D and 20B are among the highest reported when using radar satellite data over vegetated study areas. Using ERS-1 imagery, Cognard et al. (1995) compared σ_{total}^0 and θ_v in several agricultural fields in northwestern France. For vegetated fields sharing similar structural characteristics with tallgrass prairie flora, they reported correlations of $r = 0.44$ for cereal grains and $r = 0.23$ for grass pastures. In the U.K., Griffiths and Wooding (1996) also used ERS-1 data to examine the relationship between σ_{total}^0 and θ_v for three bare soil fields

and three grass fields. While bare soil correlations were high, ranging from a low of $r = 0.76$ to a high of $r = 0.99$, the relationships between σ_{total}^0 and soil moisture in the grass fields were referred to only as statistically insignificant.

More recently, Biftu and Gan (1999) estimated near-surface soil moisture conditions from RADARSAT imagery on six days for carefully selected agricultural fields, pastureland, and herbaceous rangeland sites in the Canadian province of Alberta. They indicated excellent results using linear regression, with correlation coefficients ranging from $r = 0.67$ to $r = 0.92$. Their results are stronger than those reported here, but a direct comparison is difficult given different operating characteristics of the sensors onboard the RADARSAT and ERS series of radar satellites.

Primarily because no parameter accounting for canopy or litter moisture content was used to generate simulated σ_{veg}^0 values, single linear regression equations for the burned and unburned watersheds were not adequate for predicting soil moisture over the entire study period. Rather, separate equations for areas distinguished by burning regime and image date were required. Linear regression equations derived from correlation relationships shown in figures 8 and 9 were inverted and solved for volumetric soil moisture. The mean amount of variance in θ_v explained by σ_{soil}^0 throughout the study period for the burned and unburned watersheds was $R^2 = 0.40$ and $R^2 = 0.45$, respectively (table 5).

Although the coefficients of determination between the two watersheds were similar, the total error in the regression model (RSS) for the unburned watershed was greater (34.50 vs. 22.22) for all image dates combined and for three of four dates available for direct comparison. Similarly, the standard error (SE) of the estimate was generally higher for the unburned watershed, with a mean SE for all image dates of approximately 13% for watershed 20B and 9% for

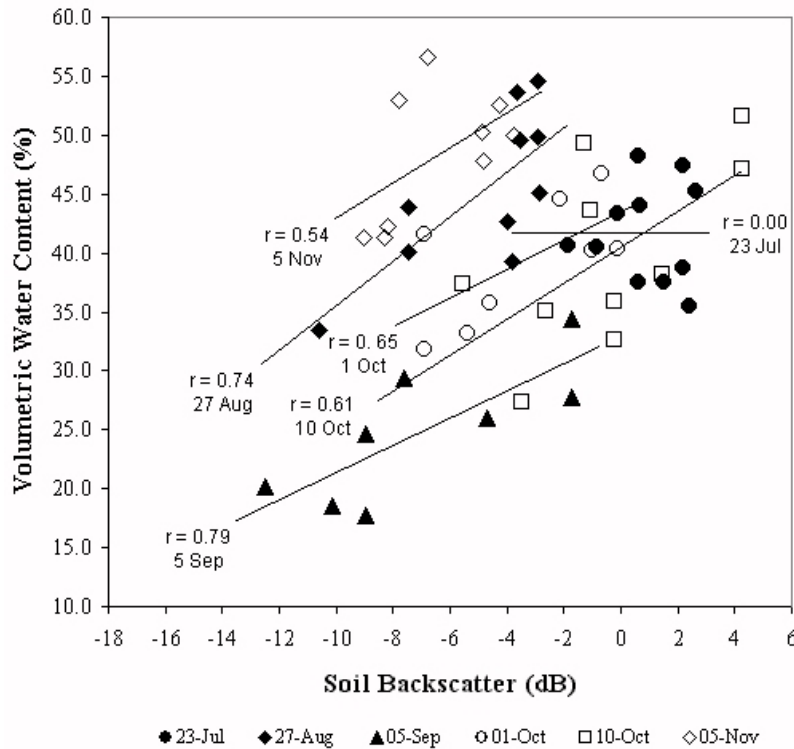


Figure 9. Correlations between soil backscatter (σ_{soil}^0) and volumetric soil moisture (θ_v) on watershed 20B (unburned) for radar image acquisition dates (1 August 1996 not shown).

Table 6. Mean and variance of σ_{total}^0 before and after topographic correction.

| Date (1996) | Before Correction | | After Correction | | Variance Difference (%) |
|----------------|----------------------|------------|---------------------|------------|-------------------------------|
| | \bar{x} | σ^2 | \bar{x} | σ^2 | |
| 23 July | -8.64 | 11.43 | -8.30 | 9.81 | -14.17 |
| 01 Aug. | -10.07 | 17.78 | -9.68 | 16.28 | -8.68 |
| 27 Aug. | -10.49 | 11.86 | -10.09 | 9.95 | -16.10 |
| 05 Sept. | -11.58 | 15.20 | -11.15 | 13.36 | -12.11 |
| 01 Oct. | -10.26 | 12.73 | -9.86 | 10.78 | -15.32 |
| 10 Oct. | -7.53 | 19.70 | -7.18 | 17.52 | -11.07 |
| 05 Nov. | -9.84 | 14.06 | -9.47 | 12.19 | -13.30 |

watershed 1D. For single dates, SE was either comparable or higher within the unburned watershed (table 5).

Regression results indicate that lack of a canopy moisture term limits the performance of the modified cloud model. Coefficients of determination for both the burned and unburned watersheds were highest during late summer (27 August and 5 September), days nearest peak canopy greenness and when NDVI-based biomass estimates would be most valid. Further, litter moisture was not a factor, as those dates were driest owing to elevated evapotranspiration rates caused by high summer temperatures, low humidity, and windy conditions. Increasing the spatial and temporal accuracy of green biomass estimates, coupled with a canopy moisture term, may extend the period for which σ_{soil}^0 is a reasonable predictor of soil moisture.

Topography also appears to negatively influence soil moisture results, despite the applied topographic correction procedure. Performance of the correction was evaluated by measuring the variance of σ_{total}^0 before and after application of the polynomial (table 6). Observed reduction of image

variance (8.4% to 16.1%) is very good for this type of correction model and compares favorably with others found in the literature (e.g., Hinse et al., 1988; Bayer et al., 1991).

After topographic correction, all dates showed a reduction in image variance and mean σ_{total}^0 value, with the polynomial function being more effective at reducing σ_{total}^0 for areas of low local incidence angles than increasing σ_{total}^0 for areas with higher angles. The increased slant range distance through vegetation at higher local incidence could be responsible for attenuating the radar signal to such a degree that a correction, based only on LIA, cannot address. As a result, the standardized residuals for sample points located in midslope portions of the two watersheds were consistently higher than those in the upland and lowland sites.

Predicted near-surface soil moisture from individual regression relationships can be merged to help form a more comprehensive understanding of soil moisture conditions across a landscape. Preliminary near-surface soil moisture maps for the entire KPBS, generated in a GIS, clearly portray distinct differences in moisture regimes within burned and unburned watersheds, as well as expected variations in near-surface soil moisture by topographic position. Through image differencing techniques, changes in soil moisture between radar image dates can also be quantified and mapped.

CONCLUSIONS AND FUTURE INVESTIGATIONS

Many studies have questioned the sensitivity of C-band radars, operating at moderate incidence angles, to near-surface soil moisture conditions. Evidence presented here, however, shows that ERS-2 data is capable of monitoring

general near-surface soil moisture conditions over highly productive vegetated ecosystems such as tallgrass prairie. This is significant in that operating characteristics of the ERS-2 sensor appear to be sufficient for estimating and monitoring soil moisture conditions over most grassland areas and for many applications. Although weaknesses in the cloud model design (i.e., biomass estimation and canopy/litter moisture term) prevented development of one equation relating σ_{soil}^0 and θ_v , single-date correlations for both the burned and unburned watersheds are among the highest yet reported using radar satellite data. Therefore, optimism may be justified for making routine spatially distributed estimates of near-surface soil moisture conditions over large grassland regions on a single-date basis.

Future research will be oriented along two major themes. One will further our understanding of the impact of topography and vegetation on the radar backscatter coefficient. Promising techniques include using principal component analysis to separate soil moisture information from other physical and biological factors that can dominate the backscatter of radar imagery (e.g., Henebry, 1997; Verhoest et al., 1998). Incorporating remotely sensed landcover information, determined using radar (e.g., Hill et al., 1999) or optical sensors, with backscatter models capable of recognizing key structural differences in landcover types, will expand the number of regions that can be studied. The second, and more urgent, of the future research themes should deal with specifying model input parameters. Of particular importance is inclusion of canopy and litter layer moisture terms in the cloud model calculations that would permit a single, and less empirical, predictive algorithm for soil moisture to be developed. However, increasing the complexity of estimation procedures should be done with caution, as the ultimate success of radar-based soil moisture estimates will be measured not only by their accuracy, but also in the reduction and simplification of input requirements for backscatter models that would encourage widespread adoption.

ACKNOWLEDGEMENTS

Funding for this research was provided through the NASA Earth System Science Fellowship program. Additional support for the purchase of ERS-2 imagery was made possible by a European Space Agency ERS research and demonstration grant. Access to the study site and availability of several descriptive datasets were provided by the Konza Prairie LTER Program (NSF BSR-9011662). Comments from four anonymous reviewers significantly strengthened the manuscript.

REFERENCES

Attema, E. P. W., and F. T. Ulaby. 1978. Vegetation modeled as a cloud model. *Radio Science* 13: 357–364.

Bayer, T., R. Winter, and G. Schreier. 1991. Terrain influences in SAR backscatter and attempts to their correction. *IEEE Trans. Geoscience and Remote Sensing* 29(3): 451–462.

Biftu, G. F., and T. Y. Gan. 1999. Retrieving near-surface soil moisture from RADARSAT SAR data. *Water Resources Research* 35(5): 1569–1579.

Briggs, J. M., and M. D. Nellis. 1989. LANDSAT thematic mapper digital data for predicting aboveground biomass in a tallgrass prairie ecosystem. In *Proc. 11th North American Prairie*

Conference, 53–55. T. B. Bragg and J. Stubbendieck, eds. Lincoln, Neb.: University of Nebraska Press.

Briggs, J. M., M. D. Nellis, C. L. Turner, G. M. Henebry, and H. Su. 1998. A landscape perspective of patterns and processes in tallgrass prairie. Chapter 15 in *Grassland Dynamics: Long-Term Ecological Research in Tallgrass Prairie*. A. K. Knapp, J. M. Briggs, D. C. Hartnett, and S. L. Collins, eds. New York, N.Y.: Oxford University Press.

Box, E. O., B. N. Holben, and V. Kalb. 1989. Accuracy of the AVHRR vegetation index as a predictor of biomass, primary productivity, and net CO₂ flux. *Vegetatio* 80(2): 71–89.

Chauhan, N., D. LeVine, and R. Lang. 1994. Use of discrete scatter model to predict active and passive microwave sensor response to corn: Comparison of theory and data. *IEEE Trans. Geoscience and Remote Sensing* 32: 416–426.

Cognard, A. L., C. Loumagne, M. Normand, P. Olivier, C. Otle, D. Vidal-Madjar, S. Louahala, and A. Vidal. 1995. Evaluation of the ERS 1/ synthetic aperture radar capacity to estimate surface soil moisture: Two-year results over the Naizin watershed. *Water Resources Research* 31(4): 975–982.

Dobson, M. C., and F. T. Ulaby. 1986. Active microwave soil moisture research. *IEEE Trans. Geoscience and Remote Sensing* GE-24(1): 23–36.

Dobson, M. C., F. T. Ulaby, and L. E. Pierce. 1995. Land-cover classification and estimation of terrain attributes using synthetic aperture radar. *Remote Sensing of Environment* 51(1): 199–214.

Eidenshink, J. C. 1992. The 1990 conterminous US AVHRR data set. *Photogrammetric Eng. and Remote Sensing* 58(6): 809–813.

Engman, E. T., and N. Chauhan. 1995. Status of microwave soil moisture measurements with remote sensing. *Remote Sensing of Environment* 51(1): 189–198.

ERDAS. 1994. *ERDAS Field Guide*. Atlanta, Ga.: ERDAS, Inc.

Freeman, C. C. 1998. The flora of Konza Prairie: A historical review and contemporary patterns. Chapter 5 in *Grassland Dynamics: Long-Term Ecological Research in Tallgrass Prairie*. A. K. Knapp, J. M. Briggs, D. C. Hartnett, and S. L. Collins, eds. New York, N.Y.: Oxford University Press.

Fung, A. K., and H. J. Eom. 1985. A comparison between active and passive sensing of soil moisture from vegetated terrains. *IEEE Trans. Geoscience and Remote Sensing* GE-23(5): 768–775.

Fung, A. K., Z. Lee, and K. S. Chen. 1992. Backscattering from a randomly rough dielectric surface. *IEEE Trans. Geoscience and Remote Sensing* 30(2): 356–369.

Goward, S. N. 1989. Satellite bioclimatology. *J. Climate* 7(2): 710–720.

Goward, S. N., C. J. Tucker, and D. G. Dye. 1985. North American vegetation patterns observed with the NOAA-7 advanced very high resolution radiometer. *Vegetatio* 64: 3–14.

Goyal, S. K., M. S. Seyfried, and P. E. O'Neill. 1998. Effect of digital elevation model resolution on topographic correction of airborne SAR. *International J. Remote Sensing* 19(16): 3075–3096.

Griffiths, G. H., and M. G. Wooding. 1996. Temporal monitoring of soil moisture using ERS-1 SAR data. *Hydrological Processes* 10(9): 1127–1138.

Henebry, G. M. 1997. Advantages of principal components analysis for land cover segmentation from SAR image series. Paper presented at the 3rd ERS Symposium (ESA), Florence, Italy, 18–21 March. Noordwijk, Netherlands: European Space Agency, Publications Division.

Hill, M. J., G. E. Donald, and P. J. Vickery. 1999. Relating radar backscatter to biophysical properties of temperate perennial grassland. *Remote Sensing of Environment* 67(1): 15–31.

Hinse, M., Q. H. J. Gwyn, and F. Bonn. 1988. Radiometric correction of C-band imagery for topographic effects in regions of moderate relief. *IEEE Trans. Geoscience and Remote Sensing* 26(2): 122–132.

- Jensen, J. R. 1983. Biophysical remote sensing. *Annals of the Assoc. American Geographers* 73(1): 111–132.
- Knapp, A. K., and T. R. Seastedt. 1998. Introduction: Grasslands, Konza Prairie, and long-term ecological research. Chapter 1 in *Grassland Dynamics: Long-Term Ecological Research in Tallgrass Prairie*. A. K. Knapp, J. M. Briggs, D. C. Hartnett, and S. L. Collins, eds. New York, N.Y.: Oxford University Press.
- Knapp, A. K. J. M. Briggs, J. M. Blair, and C. L. Turner. 1998. Patterns and controls of aboveground net primary production in tallgrass prairie. Chapter 12 in *Grassland Dynamics: Long-Term Ecological Research in Tallgrass Prairie*. A. K. Knapp, J. M. Briggs, D. C. Hartnett, and S. L. Collins, eds. New York, N.Y.: Oxford University Press.
- Kramer, H. J. 1996. *Observation of the Earth and its Environment*. New York, N.Y.: Springer.
- Laur, H., P. Bally, P. Meadows, J. Sanchez, B. Schaettler, E. Lopinto, and D. Esteban. 1998. Derivation of the backscatter coefficient sigma-nought in ESA ERS SAR PRI products. ES-TN-RS-PM-HL09, Issue 2, Revision 5b (7 September 1998). Paris, France: European Space Agency.
- Lin, D. S., E. F. Wood, P. A. Troch, M. Mancini, and T. J. Jackson. 1994. Comparisons of remotely sensed and model-simulated soil moisture over a heterogeneous watershed. *Remote Sensing of Environment* 48(2): 159–171.
- Norwine, J., and D. H. Greigor. 1983. Vegetation classification based on advanced very high resolution radiometer (AVHRR) satellite imagery. *Remote Sensing of Environment* 13(1): 69–87.
- Pultz, T. J., R. Leconte, R. J. Brown, and B. Brisco. 1990. Quantitative soil moisture extraction from airborne SAR data. *Canadian J. Remote Sensing* 16(3): 56–62.
- Rouse, J. W., R. H. Haas, J. A. Schell, and D. W. Deering. 1974. Monitoring vegetation systems in the Great Plains with ERTS. In *Proc. 3rd Earth Resources Technology Satellite-1 Symposium*, 3010–317. NASA SP-351. Washington, D.C.: NASA, Scientific and Technical Information Office.
- Saatchi, S. S., D. M. Le Vine, and R. H. Lang. 1994. Microwave backscattering and emission model for grass canopies. *IEEE Trans. Geoscience and Remote Sensing* 32(1): 177–186.
- Steyaert, L. T. 1993. A perspective on the state of environmental simulation modeling. Chapter 3 in *Environmental Modeling with GIS*. M. Goodchild, ed. New York, N.Y.: Oxford University Press.
- Townshend, J. R. G., and C. O. Justice. 1986. Analysis of the dynamics of African vegetation using the normalized difference vegetation index. *International J. Remote Sensing* 7: 1435–1445.
- Tucker, C. J. 1979. Red and photographic infrared linear combinations for monitoring vegetations. *Remote Sensing of Environment* 8(2):127–150.
- Tucker, C. J., C. L. Vanpraet, M. J. Sharman, and G. Van Ittersum. 1985. Satellite remote sensing of total herbaceous biomass production in the Senegalese Sahel: 1980–1984. *Remote Sensing of Environment* 17: 233–249.
- Tucker, C. J., H. E. Dregne, and W. W. Newcomb. 1991. Expansion and contraction of the Sahara Desert from 1980 to 1990. *Science* 253: 299–301.
- Ulaby, F. T., R. K. Moore, and A. K. Fung. 1982. *Microwave Remote Sensing: Active and Passive, Vol. II: Radar Remote Sensing and Surface Scattering and Emission Theory*. Reading, Mass.: Addison-Wesley.
- Verhoest, N. E. C., P. A. Troch, C. Paniconi, and F. P. De Troch. 1998. Mapping basin scale variable source areas from multitemporal remotely sensed observations of soil moisture behavior. *Water Resources Research* 34(2): 3235–3244.
- Yang, W., L. Yang, and J. W. Merchant. 1997. An assessment of AVHRR/NDVI-ecoclimatological relations in Nebraska, U.S.A. *International J. Remote Sensing* 18(10): 2161–2180.